Geological Quarterly, 2025, 69, 56
DOI: https://doi.org/10.7306/gq.1829

Can present-day stress orientations be determined in salt? Borehole geometry analysis from the Fore-Sudetic Homocline, Poland

Marek JAROSIŃSKI[1], Kinga BOBEK[1,] *, Marta ADAMUSZEK[1] and Rafał NASIŁOWSKI[1]

[1] Polish Geological Institute – National Research Institute, Rakowiecka 4, 00-975 Warszawa, Poland; ORCID: 0000-0003-3084-0644 [M.J.], 0000-0002-6137-9945 [K.B.], 0000-0001-7977-9528 [M.A.]

Jarosiński, M., Bobek, K., Adamuszek, M., Nasiłowski, R., 2025. Can present-day stress orientations be determined in salt? Borehole geometry analysis from the Fore-Sudetic Homocline, Poland. Geological Quarterly, **69**, 56; https://doi.org/10.7306/gq.1829

Associate Editor: Łukasz Gągała

We analyse the regional-scale orientation of present-day horizontal stresses within the Zechstein salt deposits of the Fore-Sudetic Homocline, based on an analysis of the geometry of 23 boreholes. Using six-arm dipmeter logs (SADs), we identified systematic elongation of borehole cross-sections within salt intervals. We refer to these as breakout-like structures. These elongations demonstrate remarkable consistency within local groups of boreholes and are interpreted as resulting from natural horizontal stress anisotropy, with orientations that serve as indicators of the maximum horizontal stress (S_{Hmax}). Natural differential stresses in salt of <1 MPa can result in borehole wall stress differences of up to 4 MPa. We hypothesize that the maximum shear stress acting on the borehole wall immediately after drilling (up to 32.5 MPa) is sufficient to initiate cataclastic deformation at the grain scale and to generate microcracks. These microcracks may enhance borehole convergence and pressure-solution processes at a rate proportional to the shear stress and to the density of microcracks, which leads to observable ellipticity of boreholes in salt. Natural stress anisotropy is likely driven by differential lithostatic loading due to salt's depth variations, generating horizontal pressure gradients of ~1 MPa/km instead. Another factor could be the gravitational gliding of competent layers down the slopes of salt-basement highs. These inferences are hypothetical but represent the first attempt to identify a proxy for estimating S_{Hmax} orientation in weak salt deposits at a regional scale.

Key words: Present-day stress, salt rock, deep boreholes, dipmeter tool, Fore-Sudetic Homocline.

INTRODUCTION

In recent years, research on present-day tectonic stresses has accelerated due to the development of unconventional hydrocarbon reservoirs and increasingly sophisticated methods for managing deep subsurface spaces. Salt deposits play a key role in these analyses, as they serve as preferred host rocks for underground storage caverns, both for liquid fuels and, prospectively, for hydrogen (e.g., Tackie-Otoo and Haq, 2024). Salt also constitutes an excellent sealing and isolating barrier for hydrocarbon accumulations and potential CO_2 stores (Beauheim and Roberts, 2002). However, salt layers may also pose significant engineering challenges due to their high mobility at depth (Lux, 2009).

In this study, we examined the geometry of 23 boreholes penetrating salt units within the Fore-Sudetic Homocline (FSH; Fig. 1A). It is widely acknowledged that boreholes, akin to salt caverns, are susceptible to dissolution and viscous closure, both of which can lead to substantial operational challenges. Because of their high practical relevance, borehole closure processes in salt have been the subject of numerous studies and modeling efforts (e.g., Preece, 1987; Kim, 1988; Carcione et al., 2006; Cornet et al., 2018), though these analyses have focused more extensively on caverns (e.g., Berest et al., 2001; Breunese et al., 2021; Cyran and Kowalski, 2021; Ramesh Kumar et al., 2021; Buijze et al., 2022; Fokker and Breunese, 2022). The rate of borehole closure in salt under anisotropic regional stress fields was modeled analytically by Cornet et al. (2018). However, to our knowledge, no regional-scale analyses of borehole deformation in salt have been previously published.

We examined borehole ellipticity within the Zechstein salt interval in the context of a large structural unit, the FSH. This constitutes the first attempt to evaluate this phenomenon at a regional scale. Based on six-arm dipmeter measurements, we identified depth intervals in which directional elongation of borehole diameters in salt is significant. Subsequently, the degree of borehole cross-sectional elongation was quantified, and the dominant orientation of borehole ellipticity was statistically determined. In the discussion, we explore potential causes of this phenomenon, including theoretical estimates of the relative contribution of directional creep versus dissolution effects induced by horizontal stress anisotropy. A hypothesis was formu-

* Corresponding author, e-mail: kbob@pgi.gov.pl

Received: August 5, 2025; accepted: December 2, 2025; first published online: December 31, 2025

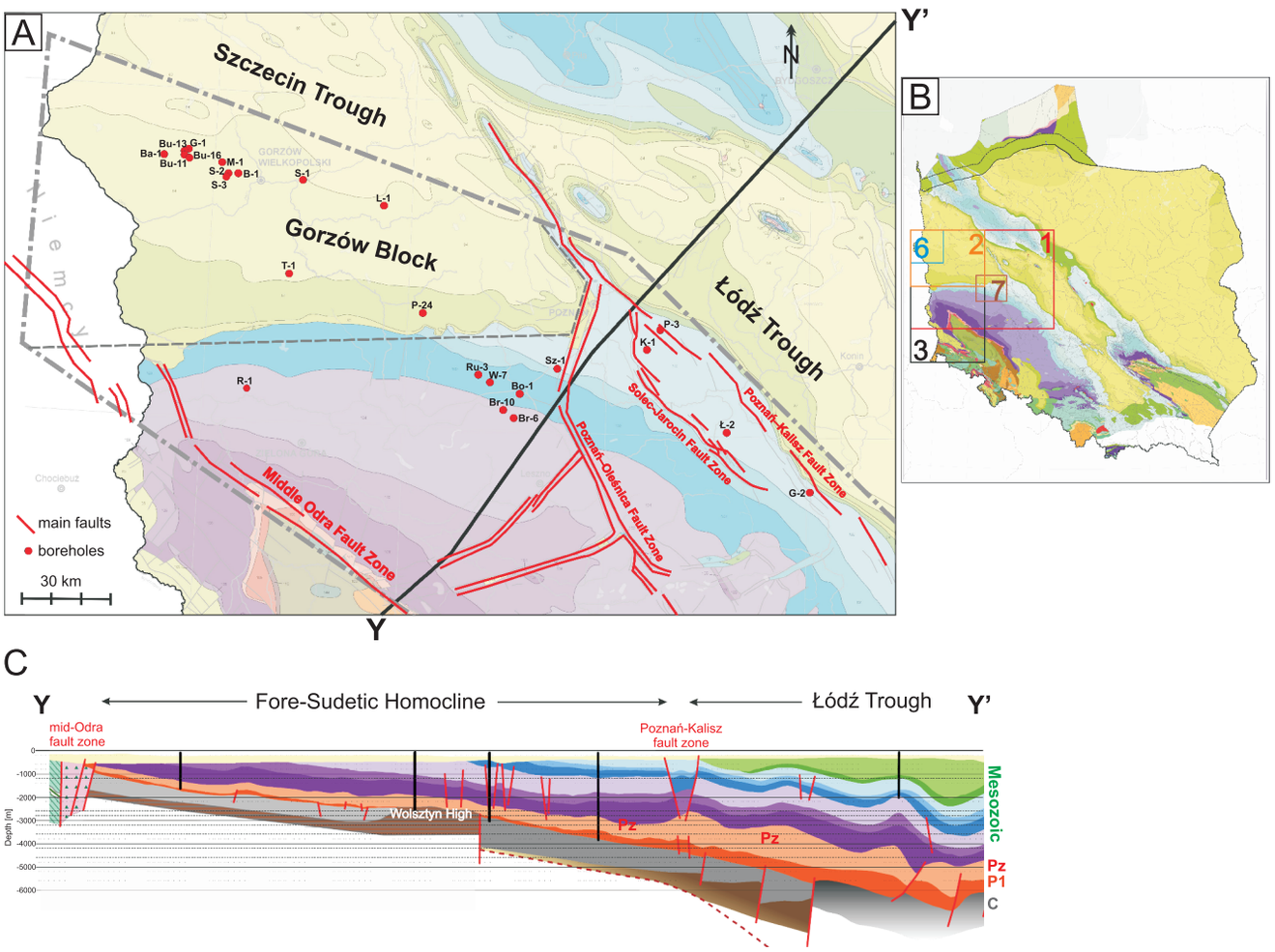

Fig. 1A – location of the boreholes analysed on the geological map of Poland excluding the Cenozoic (Dadlez et al., 2000). The black line marks the trace of the geological cross-section (Y-Y'); the grey thick dashed and dotted line outlines the extent of the FSH. A thinner, grey dashed line indicates the boundaries of the Gorzów Block. B – the area investigated, marked on the background of a map of Poland. The coloured frames with numbers refer to the areas included in particular figures in this paper. C – geological cross-section along the line marked in Figure 1A

lated that the natural stress anisotropy present in salt is attributable to the substantial pressure gradient within the salt at varying depths across the FSH.

GEOLOGICAL SETTING

The study area encompasses the FSH, a structure that formed during the Late Cretaceous (Fig. 1). During the deposition of Zechstein evaporites, this region was located at the southern margin of the Southern Permian Basin. In this basin, evaporites of four cyclothems containing salt were deposited. The Zechstein transgression advanced over an area previously covered by Rotliegend volcanic rocks and sand dunes (Kiersnowski et al., 2010; Peryt et al., 2010; Czapowski et al., 2018). On the uplifted blocks of the Wolsztyn Ridge and in the marginal parts of the basin, reef structures of the Zechstein Limestone (Ca1), and sulphate platforms (A1), developed. These structures formed several hundred-metre-high palaeotopographic highs on the evaporitic basin floor (Fig. 2). In these elevated areas, the Oldest Rock Salt (Na1) of the oldest, PZ1 cyclothem, was not deposited, although elsewhere it reaches a thickness of up to 200 m (Figs. 3 and 4). In the three subsequent cyclothems (PZ2–PZ4), the extent of the basin fluctuated near the southern boundary of the FSH, where marginal facies dominated and contained only limited amounts of salt. In the basin interior, at the locations of the boreholes studied, salt was predominantly deposited in three cyclothems, with a total cumulative thickness reaching up to 500 m. One salt layer (Na3) demonstrates its greatest thickness at the point of highest sea level within the third cyclothem, PZ3 (Fig. 3). The lowest ratio of halite facies is observed in the fourth cyclothem, PZ4, which had the smallest areal extent. The total thickness of Zechstein deposits in the area with the boreholes studied varies between 400 and 1000 m, with salt layers constituting approximately half of this thickness. However, geophysical logs from the boreholes studied often cover only a part of the complete salt profile.

Above the evaporites, a sedimentary succession with a cumulative thickness over 3 km was deposited during the Triassic, Jurassic and Cretaceous periods. The entire study area underwent a tilting event during the Late Cretaceous inversion of the Polish Basin. This event produced the homoclinal structure observed today, in which Zechstein strata generally dip towards the NNE at ~3°. Although the Zechstein deposits within the FSH region did not undergo substantial internal tectonic or halokinetic deformation, local accommodation of faults in the overburden and gentle folding of the rigid dolomite–anhydrite plate are occasionally observed.

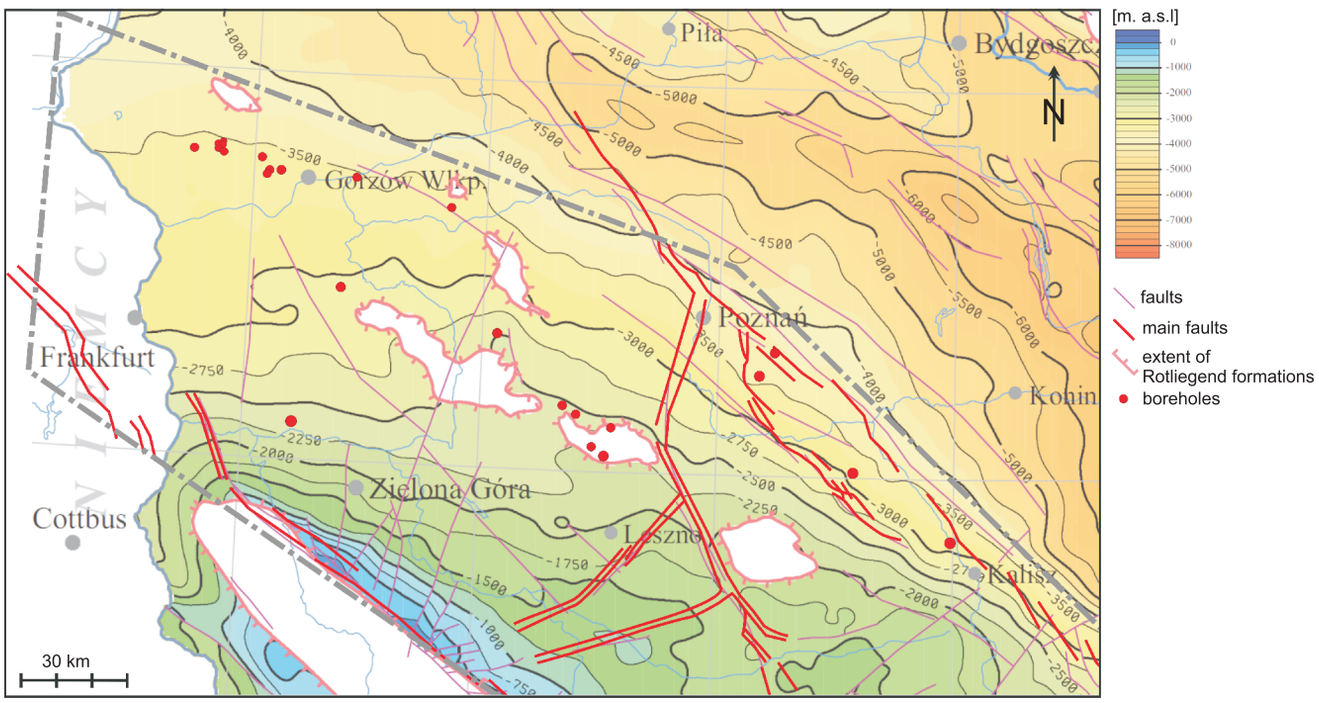

Fig. 2. Depth to the top Rotliegend surface (after Górecki et al., 2006, changed)

The white marks indicate the absence of Rotliegend strata due to the elevation of the Wolsztyn High (Fig. 3). The extent of the FSH is outlined by the grey dotted/dashed frame, and the locations of the boreholes analysed are shown as red dots

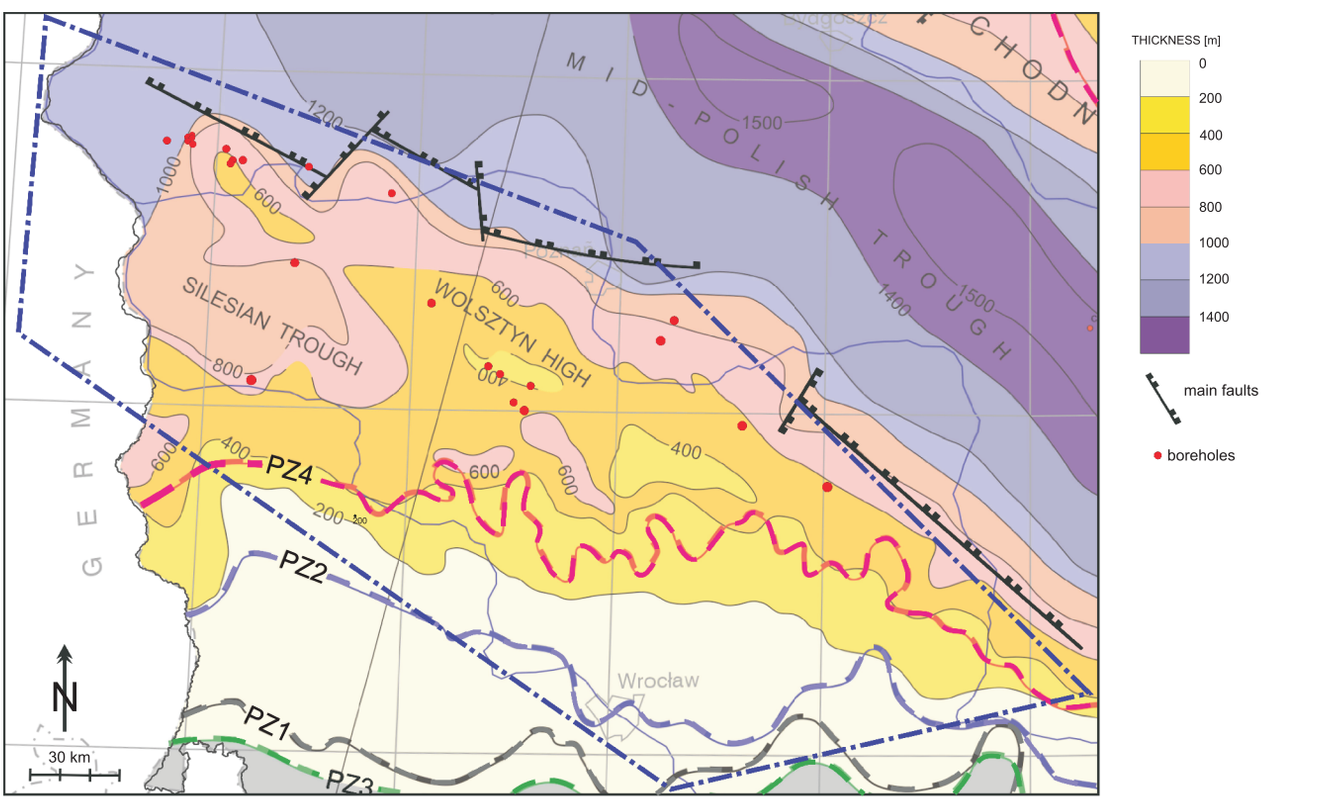

Fig. 3. The Zechstein thickness (in metres) and the extent of the four cyclothems (PZ1-PZ4; after Wagner, 1998, modified)

The FSH range is outlined by a navy blue dotted/dashed frame

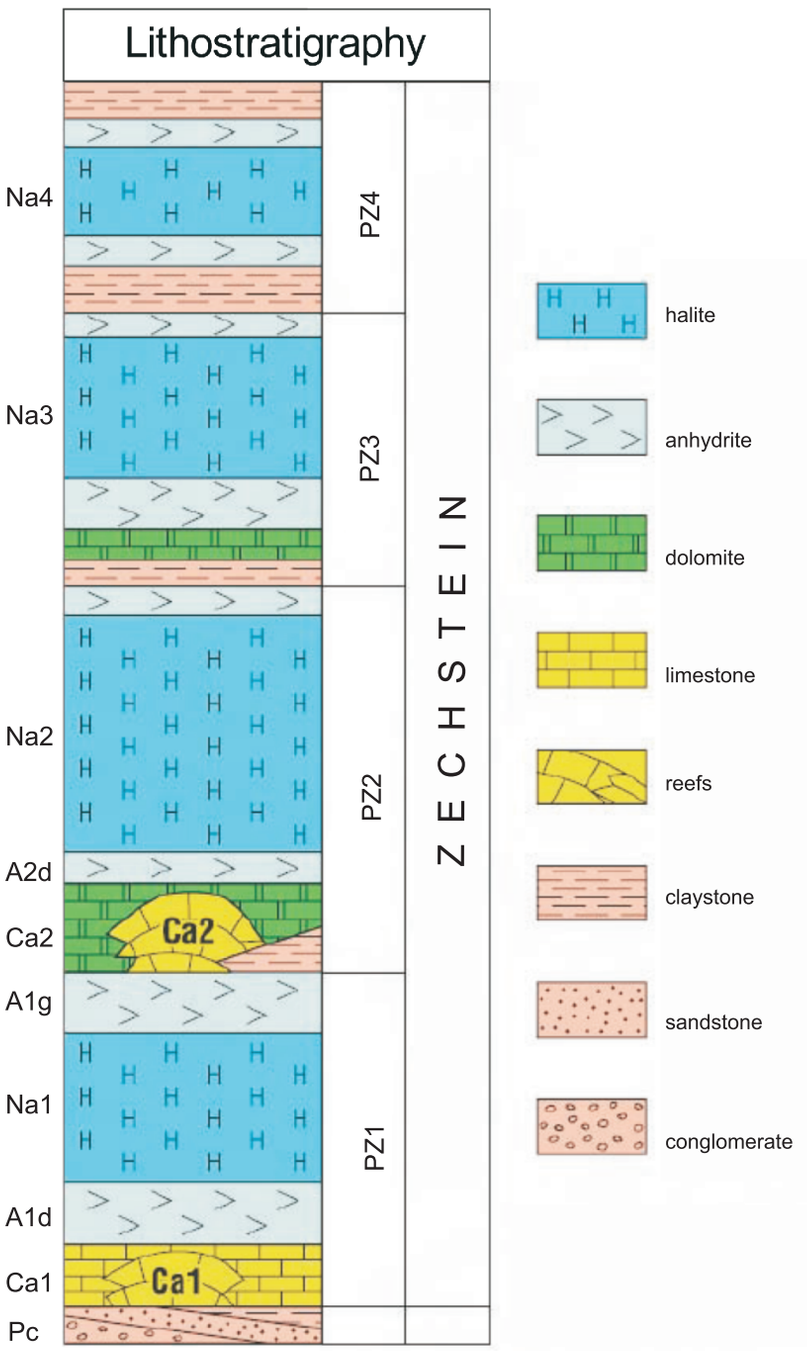

Fig. 4. Zechstein lithostratigraphic column with acronyms of units used in this paper (after Karnkowski, 1999, modified)

In contrast, in the adjacent Szczecin and Łódź troughs (to the north and north-east; Fig. 1A), salt forms pillows and diapirs, and the basal dip of the Zechstein reaches 4 and 5°, respectively. The boundaries of the FSH are defined by fault zones with post-Zechstein strike-slip displacements. In the northeast, these zones do not interrupt the continuity of salt layers between the FSH and adjacent troughs. However, in the southwest, the Middle Odra Fault Zone separates the FSH area with Zechstein deposits from the Fore-Sudetic Block, which lacks them.

Interpretations of present-day tectonic stress (S_{Hmax}) orientation based on borehole data (Jarosiński, 2005, 2006), as well as numerical stress modeling for Central Europe (Jarosiński et al., 2006), show that the regional tectonic stress is oriented NNW–SSE in this area. This configuration results from the superposition of a SE-directed ridge push originating from the Atlantic Ocean and N-directed compression from the Eastern Alps (Levi et al., 2019).

Temperature is a critical factor influencing the viscosity of salt. In the FSH region, significantly elevated heat flow values have been recorded, reaching up to 80 mW/m^2 (Szewczyk and Gientka, 2009), which correspond to temperatures at the base of the Zechstein sequence ranging from 80 to 140°C (Górecki et al., 2006). Due to the low viscosity of the salt layers and their lateral pinch-out along the southwestern margin of the FSH, the Zechstein succession appears unable to effectively transmit tectonic stresses. This interpretation is consistent with stress measurements in the substratum and overburden of the Zech-

stein, which show significant differences, suggesting mechanical detachment of stress transmission across the Zechstein evaporites.

DATA AND METHODS

The analysis of borehole geometry in salt deposits was carried out based on navigational data recorded by a Six-Arm Dipmeter Tool (SAD). This included measurements of: the lengths of the six caliper arms, the angle of the first arm relative to the borehole deviation plane, the azimuth of borehole inclination, the azimuth of the first arm, and the borehole deviation angle from the vertical (Fig. 5). In salt intervals, we analysed the orientation and degree of borehole elongation using a method previously applied to identify borehole wall enlargements known as breakouts (BB), based on algorithms from the SPIDER-6 code introduced by Jarosiński (1994, 1998, 1999). Since the origin of borehole elongation in salt is not straightforward due to the difficulty in producing brittle macro-fractures in salt (see *Discussion*), we refer to these directional elongation structures of borehole cross-sections as "**breakout-like structures"**, using the acronym **BBL** (Fig. 5).

The *SPIDER* software procedure for identifying BBL structures is based on filtering the data using two shape indicators:

- the **Asymmetry Coefficient (AC)**, which assumes the bisector of all chords of the circle will cross at its central point. If the borehole cross-section is not symmetrical, those lines will intersect at different points, creating a triangle. The size of this triangle represents the level of asymmetry, providing a quantitative measure of the asymmetry of the elongation appearing on opposite sides of the borehole walls (Fig. 5C),
- and the **Shape Coefficient (SC)**, which represents the relative difference in lengths between calipers located next to each other, quantifying the degree of cross-sectional elongation (Fig. 5D).

The definitions of these coefficients and the principles of SAD interpretation are described in Jarosiński (1998), and their effectiveness has been validated in hundreds of boreholes worldwide (performed by e.g., Baker Hughes, Geomechanics International) and numerous analyses from Poland (Jarosiński, 2005, 2006; Jarosiński et al., 2024, 2021).

To reduce noise from mechanical damage or borehole contamination, the following standard assumption is applied: BBL structures elongate the borehole diameter directionally by more than 3% (i.e., absolute SC >3%), with at least half of the elongation being symmetrical (AC >0.5). We used these threshold values to filter the data for BBL identification, but we adjusted them to more conservative values (typically SC >3.5% and AC <0.4) depending on borehole quality. This adjustment aims to achieve the clearest possible identification of elongation direction.

To account for potential artificial elongation due to side-cutting by the drill bit, which is typically associated with deviated boreholes, we also excluded data where the borehole deviation (DEVI) exceeded 3°, and the elongation direction fell within a ±20° window around the borehole inclination azimuth (HAZI). Such cases were rare because the average deviation of the boreholes analysed rarely exceeded 3°. Overall, the entire BBL structure analysis was conducted automatically, with minimal interactive adjustments to the filtering parameters.

We interpreted BBL structures in 23 boreholes, most of which are located in the northwestern part of the FSH (Fig. 1A). In these wells, the salt layers occur at depths between 2 and 3.5 km (Fig. 2), depending on their position along the monocline slope and their relationship to the above-mentioned basement highs beneath the Zechstein succession.

RESULTS

ELONGATION OF BOREHOLE CROSS-SECTIONS IN ZECHSTEIN SALT (BBL)

Upon analysing the geometry of 23 boreholes drilled through salt within the FSH, we observed that salt intervals typically show an enlarged borehole cross-section in all directions. This is due to the use of undersaturated salt solutions in the drilling mud, which are intended to prevent borehole closure in salt deposits. To quantify the degree of enlargement, we examined the difference between the minimum borehole diameter in BBL intervals and the nominal bit size (Table 1). Our analyses show that, on average, the minimum diameter is 2 cm smaller than the bit size in only one borehole, and in one case, it remains unchanged (Table 1). In the remaining wells, the minimum diameter within salt intervals exceeds the nominal bit size by an average of 10 cm, with some intervals showing differences of up to 32 cm.

Furthermore, we observed that in most salt intervals the borehole cross-section is directionally elongated along a specific axis, forming so-called BBL structures. To assess the degree of elongation (ellipticity), we used the absolute value of the shape coefficient (SC), expressed as a percentage of nominal diameter (Table 1). Elongation ranged from 6 to 15% across individual boreholes, with lower values being more frequent, resulting in an average elongation of 8% across the dataset. Because the origin of BBL structures is still under discussion, and since their geometry differs from typical breakouts, and the borehole walls are often polished (possibly by the drill string), we frequently downgraded the quality rating of the inferred S_{Hmax} direction by one, or exceptionally two points of the five-point WSMDB scale (Heidbach et al., 2025; Table 1).

All boreholes analysed boreholes are located above A1 sulphate platforms or Ca1 reef structures. Only a few boreholes encountered thin Na1 salt beds. Thus, the BBL orientations reported here mainly characterize the three thicker salt intervals. The third cyclothem (Leine) is the most widespread and thickest in the basin. In several boreholes, the BBL orientation changes slightly with depth. However, these variations are not systematic between cyclothems; therefore, the results were averaged per borehole.

Although the origin of BBL structures will be discussed later in the paper, it can already be stated that they most likely indicate the orientation of horizontal stresses in salt. As in the case of breakouts, the BBL orientation in vertical boreholes is assumed to be perpendicular to the direction of maximum horizontal stress, S_{Hmax}. We adopt this convention throughout the results section to avoid confusion that could arise from describing BBL and S_{Hmax} orientations separately. Short borehole descriptions are provided in geographical order from NW to SE. Lithostratigraphic units of the Zechstein (Pz) are labeled using the acronyms shown in Figure 4. Statistical results and spatial distribution of BBL orientations are provided in Table 1 and Figure 8.

BBL ORIENTATIONS IN BOREHOLES

Borehole **Ba-1** is located near the largest structural high of the A1 platform, which has a bifurcated shape and is penetrated by nine boreholes intersecting salt from Na4 to Na1. In the SAD log, BBL structures occur only within the uppermost part of Na2, totaling 5.25 m in length, and suggesting a NE–SW orientation of S_{Hmax}. This direction differs slightly from the NNE–SSW S_{Hmax} orientation observed in the overlying Mesozoic profile.

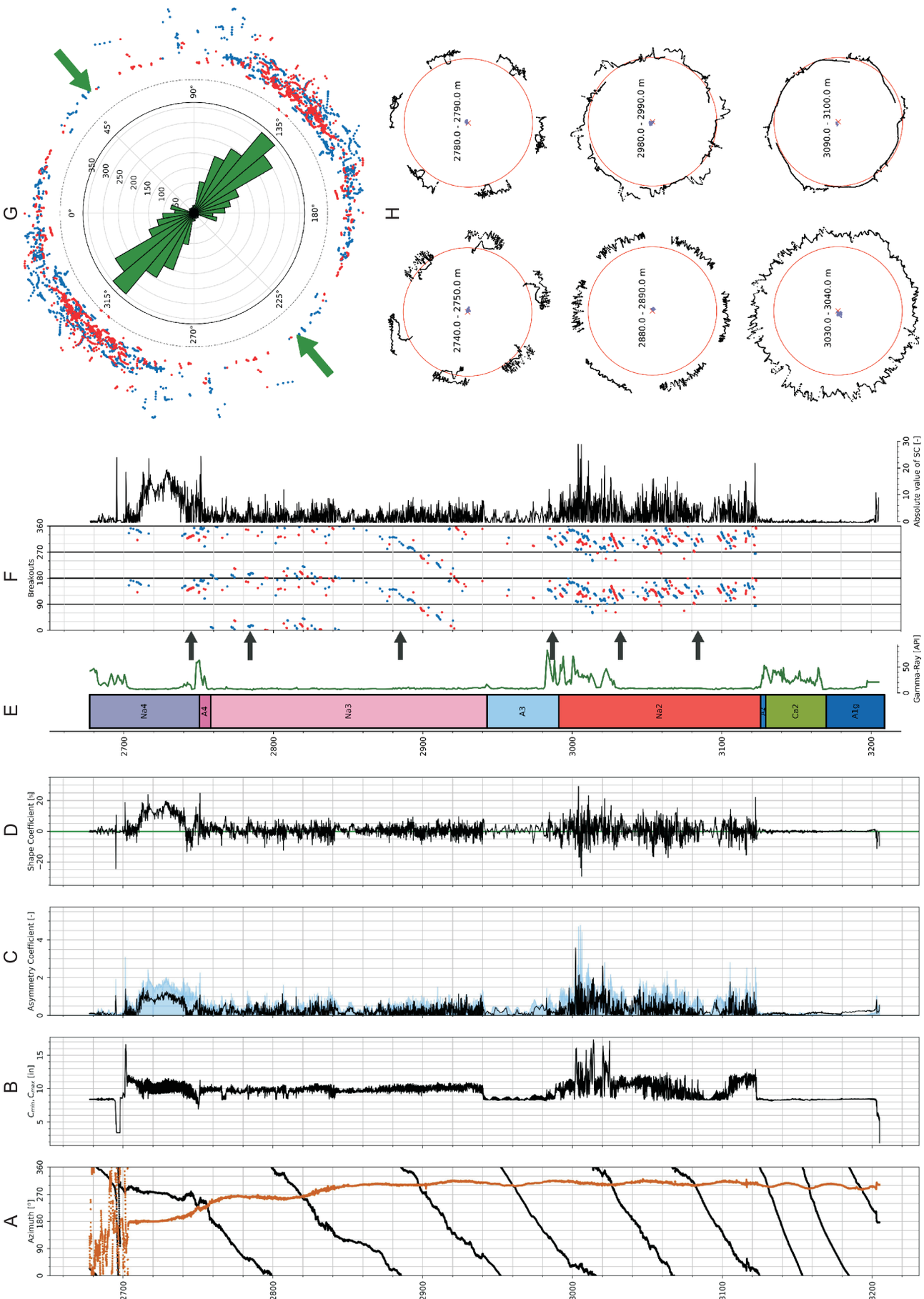

Fig. 5. Example of analyses from the Bu-16 borehole. In successive columns

A – tool rotation (black), hole azimuth (brown); **B** – the difference between caliper maximum and caliper minimum (black fill); **C** – asymmetry Coefficient (black), caliper difference (blue); **D** – shape Coefficient, positive – one caliper in BBL, negative – two calipers in BBL; **E** – lithostratigraphic column with gamma ray log (green line); **F** – interpreted BBL structures and their orientation (blue dots indicate one caliper in BBL, red dots – two calipers in BBL) with absolute values of Shape Coefficient; **G** – rose diagram of BBL (dots as in 6 column) and mean S_{Hmax} orientation (green arrows); **H** – caliper projections for selected 10 m depth intervals illustrating borehole shape variations. Black arrows on the left side of the breakout profile (F) pointing at the depth interval of the presented cross-sections (H). Results of statistical analysis are given in Table 1

Table 1

Results of the BBL analysis in salt, organized according to WSM DB standards (Heidbach et al., 2025)

Borehole	Depth interval [m]	BBL Length [m]	Mean BBL Depth [m]	S_{Hmax} Azimuth [°]	Stand. Devi. [°]	Quality	Shape Coeff. [%]	C_{min} – BS [cm]
B-1	2767–3115	11.5	2962	48	25	E	6	6
Ba-1	2599–3045	5.3	2853	52	24	E	9	-2
Bo-1	2038–2412	49.7	2143	137	9	C=>D	7	31
Br-6	1864–2133	8.9	1931	9	15	E	6	5
Br-10	1890–2155	40.8	1955	47	10	C=>E	9	9
Bu-11	2704–3120	72.6	2961	63	14	C=>D	13	0
Bu-13	2724–3120	48.7	2921	67	17	C=>D	7	1
Bu-16	2677–3126	47.4	2971	50	20	C=>D	7	5
G-1	2741–3131	51.3	2904	87	15	C=>D	8	2
G-2	2861–3115	9.8	2931	170	17	E	7	6
K-1	2920–3547	41.3	3148	62	15	C=>E	7	3
L-1	2696–3425	21.5	3079	172	21	D	8	18
Ł-2	2700–3163	47.1	2800	168	13	C->D	13	9
M-1	2713–3233	25.2	2939	44	20	D	7	7
P-24	2221–2642	21.1	2321	17	18	D	6	32
P-3	2910–3736	31.9	3163	67	15	C=>D	6	9
R-1	1707–2338	38.1	1864	74	18	C=>E	7	6
Ru-3	2163–2544	28.1	2208	22	13	D	8	29
S-1	2748–3567	61	2878	20	15	C=>D	6	26
S-2	2776–3198	55.4	2961	64	13	C=>E	6	3
S-3	2756–3262	25.4	2981	59	26	D->E	7	10
T-1	2419–2910	51.7	2529	66	13	C=>D	15	13
W-7	2063–2424	12.5	2198	167	14	E	7	5

Shape Coefficient is a measure of borehole cross-section elongation. In many cases, the WSM DB quality ranking was subjectively downgraded due to irregular borehole cross-section elongation, C_{min} – caliper minimum, BS – bit size

The next three boreholes — **Bu-11, -13, and -16** — are also located above the same A1 platform. The platform here is >200 m thick and its ENE–WSW-trending edge is bordered by normal faults that indicate gravity-driven downslope sliding of the Zechstein succession. In **Bu-11**, the SAD log covered almost the entire Zechstein profile, allowing comparison of BBL orientation across salts of four cyclothems. In **Na4**, BBL structures show consistent orientation, indicating S_{Hmax} in the ENE–WSW direction. In **Na3**, orientations range from NE–SW (in intervals with strong borehole washouts) to E–W (in narrower sections). In the 130 m-thick interval of **Na2**, BBLs suggest S_{Hmax} trending ENE–WSW. A single BBL in **Na1** also indicates this orientation. In total, BBL structures spanning 77 m point to an average S_{Hmax} orientation of ENE–WSW. Due to limited control over the exact geometry of borehole elongation, we downgraded the data quality from C to D. This S_{Hmax} direction differs significantly from the NNE–SSW compression inferred in Ca2 but aligns with the elongation axis of the A1 platform and the nearby fault trend (Fig. 6).

Bu-13 is located on the same A1 platform as the previous boreholes, but farther from its edge and away from fault zones. The SAD log covers all salt-bearing cyclothems. In Na4 and the upper part of Na3, long and regular BBL structures indicate a stable S_{Hmax} NE–SW orientation. Below, within Na3 and Na2, BBLs also indicate a stable ENE–WSW orientation. These BBL orientation ranges are similar to those from **Bu-11**, located ~1.5 km away, with an average S_{Hmax} of ENE–WSW. Due to possible partial smoothing of BBLs by the drill string, the quality rating of the stress orientation was downgraded from C to D.

Bu-16 is situated closer to the platform edge (~0.5 km). The SAD log covers three salt cyclothems (excluding Na1). In Na4 and the upper part of Na3, BBLs show a relatively stable S_{Hmax} direction of ENE–WSW. In the lower A3 and Na2, BBLs on a stable borehole wall indicate a NE–SW orientation, with the best-developed BBLs in the basal salt suggesting S_{Hmax} toward NNE–SSW. The average S_{Hmax} across the borehole is close to NE–SW, similar to the previous boreholes.

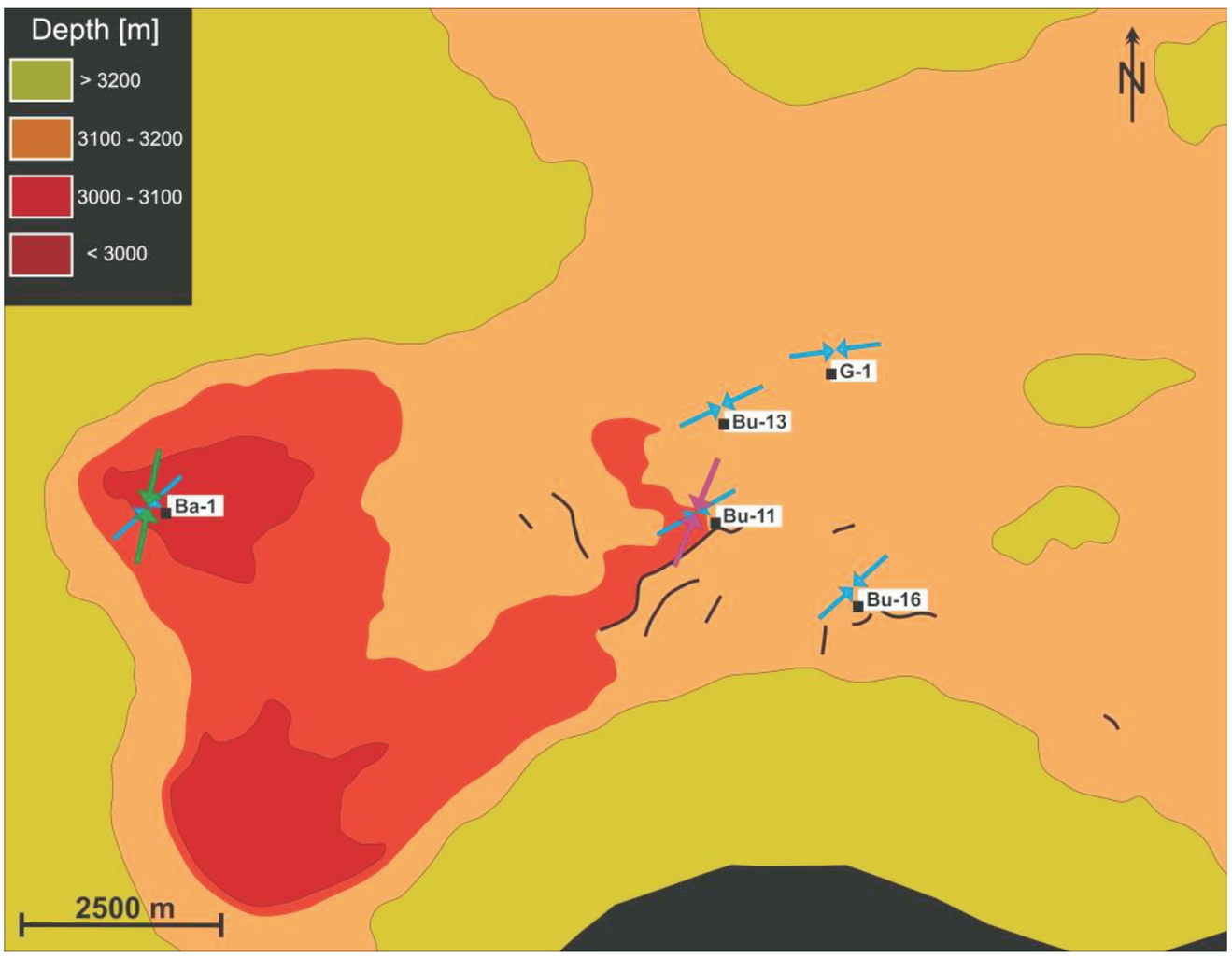

Fig. 6. Boreholes from the Ba and Bu fields shown on a map of the Z2 seismic horizon, corresponding to the top of the Ca2 unit (after Górski et al., 1999)

A clear discrepancy is visible between the consistent S_{Hmax} direction in Na2 salt (blue arrows) and the S_{Hmax} direction in the Ca2 unit (purple arrow) as well as in the Mesozoic succession (green arrow in westernmost borehole)

G-1, located on the same A1 platform as the Buszewo boreholes (with no Na1 salt), displays BBLs in Na4, Na3, and Na2 that consistently indicate an E–W S_{Hmax} orientation. The total BBL length is 51 m. This orientation aligns with the elongation axis of the platform. Due to the drill string polishing most BBLs, the measurement quality was downgraded from C to D.

M-1, also located on the same A1 platform (height ~65 m), was logged in three salt cyclothems. A bimodal BBL orientation pattern was interpreted from 25 m of structures, with average S_{Hmax} trending NE–SW or NNE–SSW, consistent with the regional monocline dip. The BBLs were not visibly polished.

S-2 sits atop the same A1 platform (height ~55 m). The SAD log covers two salt cyclothems. Near the A3–Na2 boundary, borehole elongation resembles typical breakouts—likely due to the mixed salt–anhydrite lithology. In other intervals, elongations are gentle and do not disturb tool rotation. Across both cyclothems (PZ2 and PZ3), 55 m of BBLs with variable orientation point to S_{Hmax} in the range NE–SW to E–W, averaging ENE–WSW. Due to heavy wall polishing, quality was downgraded from C to E.

S-3, also on the same platform, was logged in three salt cyclothems. All intervals are uniformly eroded. BBLs show bimodal orientations, changing within the same NE–SW to E–W range as in the adjacent borehole, with a statistical average of ENE–WSW S_{Hmax}.

B-1, located on the same A1 platform, penetrates three salt cyclothems (excluding Na1). The borehole diameter was enlarged by 3–6 cm depending on direction. BBL orientation is unstable, with an average S_{Hmax} of NE–SW based on just 11.5 m of BBL and a high standard deviation (25°), yielding the lowest quality rating (E).

S-1, located in the eastern portion of the A1 platform (thickness: 260 m), was logged across three salt cyclothems and the upper Rotliegend interval. Shallow wall washouts in Na4, Na3, and Na2 show regular elongation, suggesting S_{Hmax} of N–S in Na4, NNE–SSW in Na3 and Na2, with deeper intervals rotating further to NE–SW. The average S_{Hmax} from 61 m of BBL is NNE–SSW. Due to alignment with HAZI (though with low deviation), quality was downgraded from C to D.

L-1, also in the eastern part of A1, was logged across four salt cyclothems. In Na4, Na3, and Na2, tool rotation was smooth, and BBLs show gradual S_{Hmax} rotation with depth from NNE–SSW to N–S. In Na1, a deeper BBL that disrupted tool rotation suggests S_{Hmax} towards NNW–SSE. Overall, a bimodal S_{Hmax} pattern is observed from top to bottom, averaging N–S over 33 m of BBL.

T-1, located in the southern Gorzów Block on the same A1 platform (height: 180 m), was logged across two salt cyclothems. The borehole diameter was uniformly enlarged by

~5 cm. The most regular BBLs (totaling 52 m) indicate S_{Hmax} towards the NE–SW. Due to uncertainty in defining the elongation nature, the quality was downgraded from C to D.

P-24, on the southern edge of the Gorzów Block atop an approximately 90 m thick A1 platform trending WNW–ESE (north of the Ca1 reef), was logged between 2221–2642 m depth across two salt cyclothems. Wide washouts in Na3 and Na2 increased borehole diameter by 10–15 cm. BBLs in these intervals suggest S_{Hmax} towards NNE–SSW and, subordinately, N–S. A bimodal distribution (total BBL length: 21 m) yields an average S_{Hmax} of NNE–SSW, perpendicular to the local elongation of the A1 platform.

R-1, located above a ~250 m high A1 platform trending NW–SE, away from its flanks, pierced units from Na3 to the upper Rotliegend. In Na3 and Na2, borehole walls are heavily eroded. Well-developed BBLs indicate ENE–WSW S_{Hmax}. In the thin Ca1 interval, short BBLs suggest S_{Hmax} of NNE–SSW, while sparse breakouts in the Rotliegend suggest N–S orientation. Due to wall asymmetry suggesting drill-string polishing, quality was downgraded from C to E.

Ru-3, located in the northeastern part of the FSH's western segment, lies above the Ca1 reef (thickness: ~80 m). The SAD log covered two salt cyclothems. In Na3 and Na2, deep washouts (~10 cm) occurred. Symmetrical and distinct BBLs (totaling 28 m) consistently indicate S_{Hmax} towards the NNE–SSW.

W-7, on the eastern edge of the western FSH segment, lies atop a 110 m thick A1 platform near the flank of a Ca1 reef. The SAD log includes Na2 and Na3, with BBLs at A3–Na2 and less frequently at the Na3–A3 and Na2–A2 boundaries. The total BBL length of 12.5 m suggests S_{Hmax} of NNW–SSE, similar to N–S orientations indicated by sparse breakouts in the Carboniferous.

Bo-1, at the eastern limit of the western FSH segment, lies above a ~90 m high Ca1 reef. The SAD log includes two salt cyclothems and Carboniferous strata. Regardless of whether the borehole wall is polished or not, BBLs totaling 50 m consistently indicate NW–SE S_{Hmax}, in agreement with the Carboniferous stress data. Due to polishing, measurement quality was downgraded from C to D.

Br-6, atop an extension of the Ca1 reef (~40 m high, trending WNW–ESE) (Fig. 7), was logged in Na3 and Na2. From 9 m of BBLs, S_{Hmax} is interpreted as NNE–SSW. This orientation aligns with the dip of the FSH and reef slope and is oblique to the regional tectonic compression direction in the Zechstein substratum.

Br-10 is located above the same Ca1 reef as the previous borehole, with a height of ~48 m, situated at the crest of a structural high trending NW–SE (Fig. 7). BBL structures in Na3, totaling 48 m in length, suggest a S_{Hmax} orientation towards the NE–SW, similar to the previous borehole and aligned with the downslope direction of the reef body. Due to significant polishing of the borehole wall by the drill string, the quality rating was downgraded from C to E.

P-3 is situated within the Poznań–Kalisz fault zone, above an A1 platform ~300 m thick. The SAD log covers two salt cyclothems, but BBLs occur only in Na3. These BBLs, totaling 32 m, show unstable orientations and suggest a S_{Hmax} direction of ENE–WSW. Due to the lack of clear structural symmetry, the quality rating was downgraded from C to D.

K-1, also located within the Poznań–Kalisz fault zone, lies above a A1 platform ~230 m thick, trending NW–SE. In Na3, BBLs show unstable orientations, indicating a NE–SW S_{Hmax} direction. In Na2, more stable BBLs point to ENE–WSW S_{Hmax}. This matches the borehole average and closely aligns with the local slope of the platform. Due to polished borehole walls, this result was assigned the lowest quality rating, E.

Ł-2, located near the Poznań–Kalisz fault zone above a 65 m-thick A1 platform, shows relatively stable BBL orientations across all three salt cyclothems, with a total BBL length of 47.1 m. These structures suggest a S_{Hmax} orientation of NNW–SSE, similar to that observed in the Zechstein substratum. Given the potential for drill-string polishing, the quality rating was downgraded from C to D.

G-2 is located on the eastern edge of the FSH, within the Poznań–Kalisz fault zone, and above an A1d platform more than 120 m thick. In the intervals of Na2 and Na1, both significantly thinned, 10 m of BBLs suggest a S_{Hmax} orientation of NNW–SSE. This direction is consistent with that observed in the underlying Rotliegend. The measurement was given the lowest quality rating, E.

SYNTHESIS OF S_{HMAX} ORIENTATIONS IN SALT

In the statistical analysis of S_{Hmax} orientations from all boreholes drilled in salt (Fig. 9), the average S_{Hmax} direction for each borehole was weighted according to measurement quality: class D was assigned 2 points, and class E received 1 point. By deliberately omitting weighting by total BBL length, we avoided overemphasizing results from individual wells with exceptionally long cumulative BBL intervals. To interpret the orientations of S_{Hmax}, we compared them with the FSH dip reference direction, which we determined using a hypsometric map of the Zechstein base (Fig. 8). This surface reflects the general dip and tilt direction of the FSH after Zechstein deposition, as well as the larger irregularities in the Zechstein substratum caused by the uplift of this area or the large aeolian dunes in the Rotliegend.

A particularly noteworthy observation is that clusters of closely spaced boreholes tend to exhibit similar BBL orientations. This strongly suggests that borehole elongation is not a technological artifact resulting from drill string wall abrasion. Such artifacts are usually found in significantly deviated wells or inclined layers, neither of which are present in the current dataset. Additionally, sidewall erosion by the drill string was ruled out through filtering based on hole azimuth. If homoclinal layer dip were significantly affecting the data, we would expect to see systematic borehole elongation in the NNE–SSW direction. However, this pattern is absent from all boreholes analysed.

The most striking example of systematic BBL orientation comes from S_{Hmax} analysis in nine closely spaced boreholes located within the Gorzów Block (northern part of the FSH), all situated above a single A1 anhydrite platform (Fig. 8 and Table 1). These wells display similar BBL orientations, indicating a consistent ENE–WSW S_{Hmax} direction. A comparable S_{Hmax} orientation was also observed in two boreholes located south of this platform and in three additional boreholes in the eastern part of the FSH, including two near its northeastern margin. In contrast, six boreholes situated in the western FSH segment above the Ca1 reefs – as well as **L-1** and **S-1** – show S_{Hmax} directions aligned with the dip of the FSH and the slopes of nearby platform edges.

In total, 806 metres of BBL structures were identified across 23 boreholes, all potentially suitable for characterizing S_{Hmax} orientation in the salt. Statistically, we observed a dominant S_{Hmax} azimuth at 60°, with a mean orientation ~47°. This offset results from a consistent left-lateral deviation in most remaining measurements relative to the dominant direction (Table 1). These results do not clearly indicate a direct correlation between S_{Hmax} orientation and the dip of the FSH (Fig. 2). However, the mean S_{Hmax} direction deviates by only ~25° from the general FSH dip. In many boreholes, S_{Hmax} was observed to align with the slope

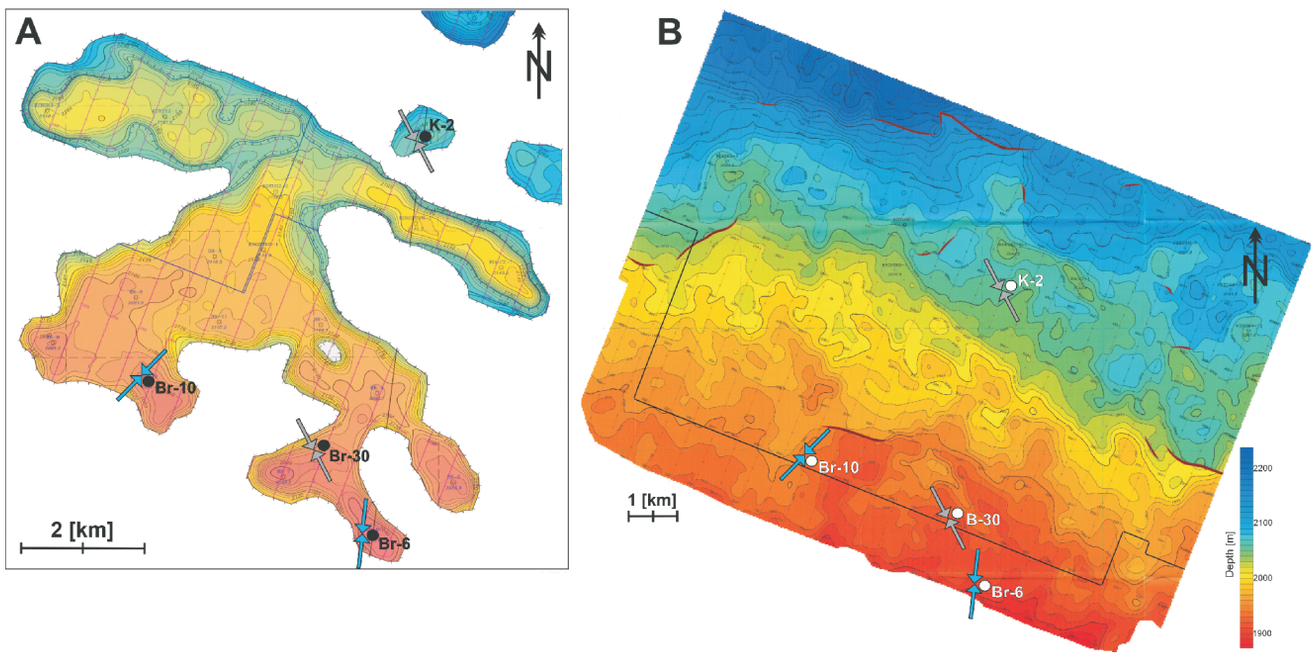

Fig. 7. Maps: (A) top of the Ca1 unit (reef of the Zechstein Limestone), and (B) Z2 seismic horizon corresponding approximately to the top of the Ca2 unit (Zdanowski and Solarski, 2018)

A clear difference is visible between the S_{Hmax} orientation in salt (blue arrows), which is perpendicular to the edge of the Ca1 high, and the S_{Hmax} orientation in the Carboniferous basement (grey arrows)

of underlying reef or platform structures. Only in one case did we identify a S_{Hmax} orientation perpendicular to both the monocline dip and local topographic gradient.

DISCUSSION

CAUSES OF BOREHOLE CROSS-SECTION ELONGATION IN SALT

In all salt intervals of the boreholes studied, we consistently observed borehole diameter enlargement in all directions, clear evidence of salt dissolution by undersaturated (with respect to NaCl) drilling mud. However, our analysis focuses specifically on the causes of directional elongation of borehole cross-sections within the salt.

This well-documented phenomenon in rocks other than evaporites involves shear stress concentration around the borehole wall. This results in compressive failure and the formation of breakouts aligned with the direction of minimum horizontal stress (S_{hmin}). When the shear stress exceeds the uniaxial compressive strength of the rock around the entire perimeter of the borehole, the cross-section enlarges while maintaining its elongation in the S_{hmin} direction. To determine if analogous breakout-like structures can form in salt, we must examine the mechanical and stress-related factors of Zechstein salts in the FSH.

Stress and deformation conditions in salt within the FSH

Within the FSH, salt layers represent the weakest rheological components, and may act as mechanical detachment levels between the Paleozoic Zechstein substratum and its Mesozoic overburden (Jarosiński, 2006; Jarosiński et al., 2021). The greater the depth and temperature, and the lower the strain rate, the less brittle and elastic salt or anhydrite becomes, with creep becoming the dominant deformation mechanism (Jackson and Hudec, 2017).

In the boreholes analysed that penetrate the salt, the base of the Zechstein lies at depths between 2 and 3.5 km (Fig. 2), with most boreholes reaching close to 3 km. At these depths, temperatures range between 80–140°C, with the typical value ~100°C. The present-day tectonic horizontal strain rate for the monocline has been estimated at $10^{-16}s^{-1}$ (Araszkiewicz et al., 2016). However, we argue that salt does not directly participate in tectonic deformation; instead, its mechanical behaviour is likely governed by gravitational effects resulting from differences in lithostatic pressure between areas of varying depth within the FSH.

Stress measurements suggest that both the Mesozoic overburden and dolomite–anhydrite interbeds within the salt may undergo gravitational creep either along or within the salt layers. This movement is driven by the monocline dip and the density contrast between anhydrites/dolomites and salt. It is therefore plausible that gravity contributes to locally increased strain rates at material boundaries within the salt. Under a strain rate of $10^{-14}s^{-1}$, it can be inferred that dry rock salt under these conditions would support differential stresses below 2 MPa at 80°C and below 1 MPa at 120°C (Jackson and Hudec, 2017). Since such high strain rates are likely unrealistic in natural settings, we conclude that natural differential stresses in the FSH salt probably do not exceed 1 MPa.

MECHANISMS OF BOREHOLE CROSS-SECTION ELONGATION IN SALT

The development of oval shapes of boreholes in salt deposits results from local variations in the magnitude and orientation of the stresses acting on the borehole wall. Immediately after drilling, before the viscoelastic stress relaxation mechanism in salt becomes active, the vertical stress at the borehole wall equals the lithostatic pressure, while the borehole wall is supported solely by the mud fluid pressure. For the depth range considered in this study (2–3.5 km) and assuming an average

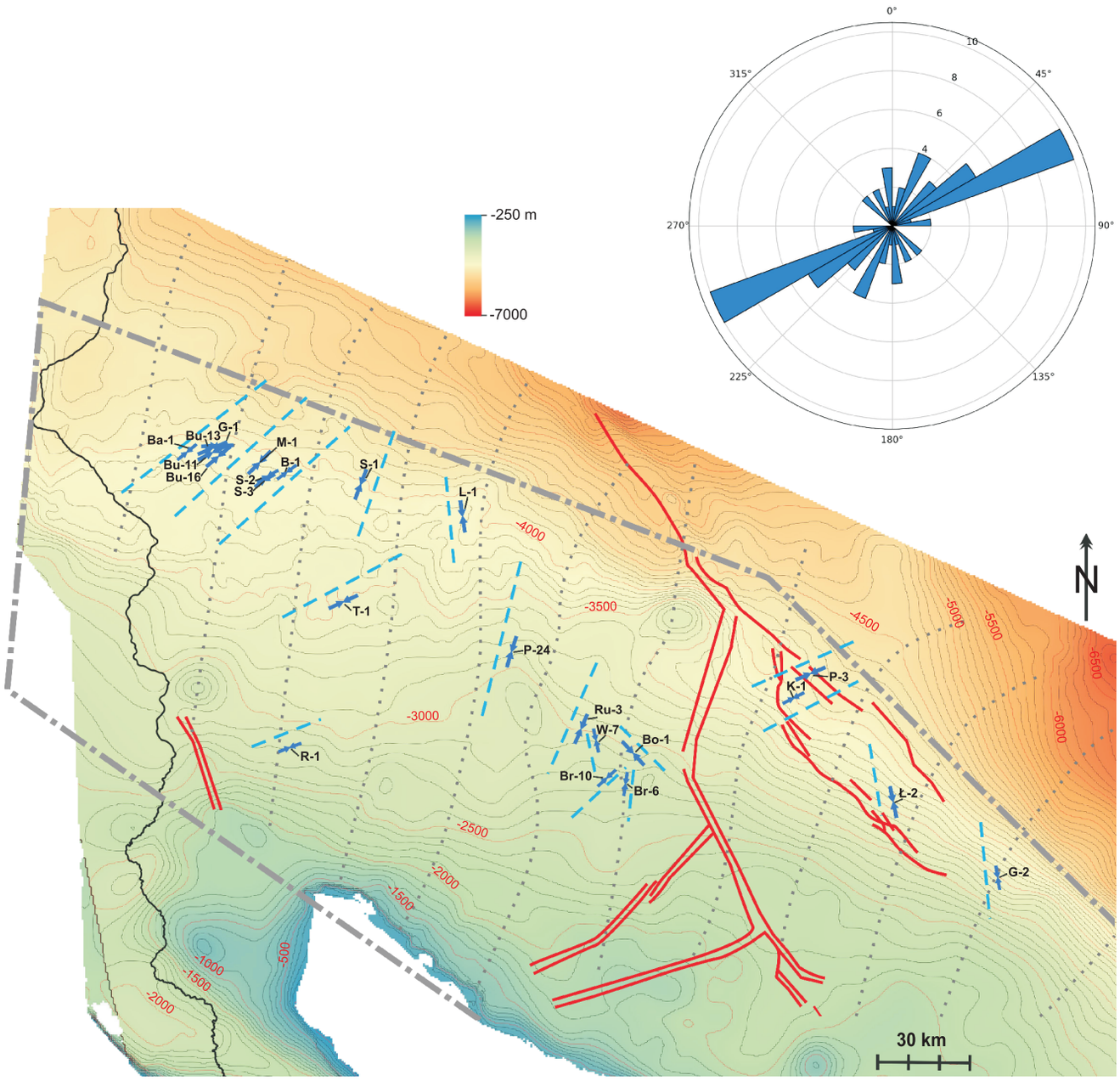

Fig. 8. Average S_{Hmax} directions for the salt intervals (Na1, Na2 and Na3, combined) in the boreholes analysed (blue arrows), highlighted by the local S_{Hmax} trajectory trends (blue dashed lines)

In the background, a hypsometric map of the Zechstein base with 100 m contour intervals (thin grey lines) and indicated slope lines of this surface (grey dotted lines). The rose diagram shows the S_{Hmax} orientation statistics for all boreholes shown, weighted by measurement quality

overburden density of 2.4 g/cm^3, the lithostatic pressure ranges from 48 MPa to 84 MPa. Due to elevated pore pressure in the Zechstein salt at greater depths (Bojarski, 1997), the mud weight was adjusted and varied between 1.3 g/cm^3 for shallow wells and 1.5 g/cm^3 for deeper ones. This results in a borehole pressure (P_m) ranging from 26 MPa to 52.5 MPa, respectively. Consequently, the maximum differential pressure between lithostatic and borehole pressures ranges from 22 MPa to 31.5 MPa, depending on the borehole depth. This pressure difference leads to transient shear stress in the borehole wall. However, due to the anisotropy of in-situ stress in salt, the circumferential stress around the borehole wall (S) varies with the angle between the direction of S_{Hmax} and the measurement point on the borehole wall (, measured from the borehole axis), and can be described using the classical Kirsch equation (Kirsch, 1898, Eq. 1):

$$S = S_{Hmax} + S_{hmin} - 2(S_{Hmax} - S_{hmin}) \cos 2 - P_m \quad [1]$$

Below, we focus on the maximum and minimum circumferential stresses in the directions S_{Hmin} and S_{Hmax}, respectively. For a depth of 2 km, this yields values of S_{max} = 72 MPa and S_{min} = 68 MPa, which gives a maximum shear stress of: (S_{max}

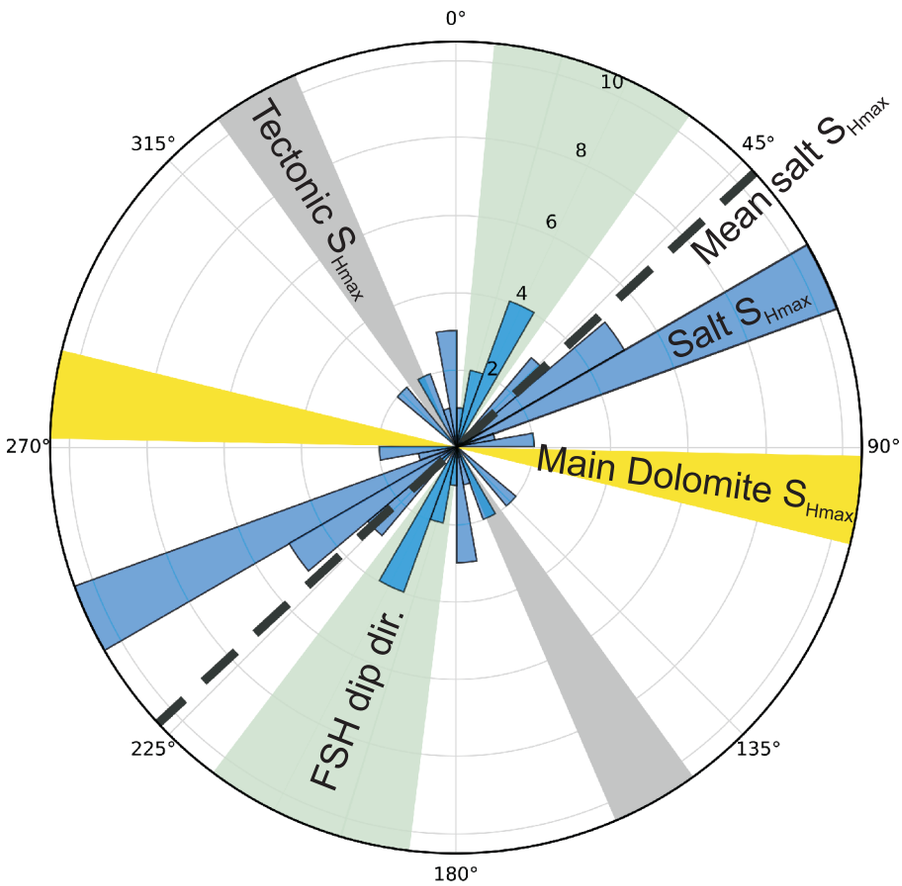

Fig. 9. Directions of S_{Hmax} salt (blue) compared with tectonic stress in the Carboniferous basement (grey), S_{Hmax} in the Main Dolomite (yellow) and the FSH dip direction (green)

$- P_m)/2 = 23$ MPa. At a depth of 3.5 km, the values are $S_{max} = 117.5$ MPa and $S_{min} = 113.5$ MPa, yielding a maximum shear stress of: $(S_{max} - P_m)/2 = 32.5$ MPa. This stress state only exists temporarily, until it is relaxed by viscous salt creep. Under elevated differential stress at the borehole wall, creep deformation accelerates significantly compared to natural long-term strain rates.

Accounting for the compressive strength of salt allows for the assessment of whether the transient peak stress conditions in the borehole wall may cause the formation of breakout structures. Results of uniaxial compressive strength (UCS) tests on salt samples from the FSH conducted at room temperature show that UCS values range from 17 to 34 MPa (Flisiak, 2008; Kłeczek and Zelias, 2012; Cyran et al., 2016). These values are comparable to the maximum shear stresses estimated for shallow and deep wells, respectively. However, in the borehole wall, strength is significantly influenced by borehole fluid pressure.

Triaxial strength experiments on salt from the FSH conducted under confining pressures of up to 30 MPa (Flisiak, 2007) indicate that salt strength increases significantly, reaching up to 75 MPa at 2 km depth. Since no tests have been performed for higher confining pressures, we extrapolate the observed trend linearly. For a mud pressure corresponding to a depth of 3.5 km, the estimated shear strength of salt exceeds 125 MPa. This suggests that the compressive strength of salt at the depths studied may be up to three times higher than the maximum shear stresses acting at the borehole wall. Hence, macroscopic failure in the form of breakouts is unlikely to occur in the salt. However, we argue that cataclastic deformation in the crystalline salt cannot be excluded, potentially leading to the formation of microcracks (e.g., Cristescu and Hunsche, 1998). Such microcracking could influence both the rate of deformation (Ghanbarzadeh et al., 2015) and the rate of salt dissolution along the borehole wall (Falcon-Suarez et al., 2024). Nevertheless, differences in the rates of these processes along different directions are expected to be small. As we have shown, assuming a natural stress anisotropy of $(S_{Hmax} - S_{hmin}) = 1$ MPa, the maximum circumferential stress difference in the borehole wall is no more than 4 MPa, regardless of borehole depth.

We can evaluate what percentage of the average circumferential stress is represented by this maximum differential stress using the following equation (Eq. 2):

$$E \frac{2 S_{max} S_{min}}{S_{max} S_{min}} \quad [2]$$

This calculated circumferential stress "ellipticity" ranges from 5.7 to 3.5% for borehole depths of 2 and 3.5 km, respectively. These values are only slightly lower than the observed ellipticity of the borehole cross-sections (Table 1), which averages ~8%. However, we do not assign strict physical meaning to this coincidence.

We hypothesize that the elliptical shape results from variations in the direction of microcrack density, which are likely proportional to the magnitude of shear stress at the borehole wall. This could proportionally increase the rate of pressure solution and localized borehole wall enlargement. Pressure solution would promote faster enlargement of the borehole diameter in the S_{hmin} direction. The presence of secondary phase impurities in the halite, such as anhydrite and clay, enhances dilatancy and thus permeability (Beauheim and Roberts, 2002), further facilitating fluid penetration along microcracks. Meanwhile, anisotropic compressive stress would lead to convergence of the borehole wall in the S_{Hmax} direction. Ultimately, both mechanisms contribute to borehole elongation in a direction typical of breakouts. Therefore, we refer to such elongations in salt deposits as BBLs (breakout-like structures). Since the minimum borehole diameter is only below the nominal value in one case, we infer that dissolution dominates closure rate. Finally, high circumferential stresses in the borehole wall preclude tensile microfracturing, despite the low tensile strength of salt.

DIRECTIONAL BOREHOLE CLOSURE

The closure rate of boreholes in rock salt is a highly non-linear process influenced by numerous interacting factors (Morales Salazar, 2024). A key role is played by the dominant creep mechanism: under low regional stress and fine-grained salt structure, diffusion creep prevails, whereas under high stress conditions and coarse-grained textures, dislocation creep becomes dominant (Li and Urai, 2016). In the depth range typical for the boreholes studied (>2 km; Table 1), diffusion creep is generally the prevailing mechanism, indicating strong strain-rate sensitivity to grain size. Elevated temperature and the presence of shear stresses significantly accelerate the borehole closure rate, by several orders of magnitude. The analytical model developed by Carcione et al. (2006) demonstrated that differential horizontal stresses lead to elliptical deformation of boreholes, with deformation governed by stress anisotropy, temperature, and the viscoelastic rheological properties of salt. These dependencies are also well captured in the model proposed by Cornet et al. (2018), which integrates pressure solution and dislocation creep under anisotropic regional stress conditions, allowing rapid estimation of deformation rates as a function of geothermal and geomechanical parameters.

Using the model of Cornet et al. (2018), we estimated that for a borehole with radius R = 0.105 m, and a lithostatic-to-hydrostatic pressure difference of 20–30 MPa, under elevated temperatures of up to 140°C (in the deepest boreholes) and fine-grained salt texture (grain size d = 0.5–1 mm), the closure rates may reach several centimetres per month, implying that observable deformation can occur within just a week. The results align with field observations from salt drilling operations, where radial closure has been shown to become critical within hours or days under similar conditions of high differential stress, elevated temperature, and fine-grained salt microstructure (e.g., Munson and Dawson, 1980; Dusseault et al., 2004; Carcione et al., 2006). Conversely, at lower temperatures and with coarser grain size, the strain rate clearly decreases. However, when microcracking occurs in the borehole wall, the deformation rate may increase further. The case we consider, namely borehole wall deformation under significantly elevated shear stresses and in the presence of undersaturated borehole fluids penetrating microcracks, differs from the creep-driven salt deformation scenarios previously studied. Therefore, for the purpose of this analysis, we refrain from modeling of borehole ellipticity controlled by the creep mechanism.

PRESSURE DISSOLUTION

Another potential cause of directional elongation of the borehole cross-section is pressure solution, which accelerates the dissolution rate under increased shear stress in the borehole wall. Under such stress, Na^+ and Cl^- ions are mobilized from more heavily loaded grain contacts and transported along water films toward zones of lower pressure (Spiers et al., 1990). The highest shear stress in the borehole wall occurs in the direction of S_{hmin}, which may also correspond to the highest intensity of microcracking. These structures provide preferred sites for salt precipitation. In this way, the process of creep in salt can be initiated and directionally enhanced.

In the presence of direct contact with the borehole wall, the process may become more complex. An undersaturated mud filtrate can enhance salt dissolution and prevent its precipitation, thereby accelerating the solution rate. As such, this mechanism may be more effective than the classical creep mechanism driven by pressure-solution–precipitation processes in salt (Urai et al., 1986). However, pressure solution in the presence of an undersaturated fluid has not yet been quantified. Related mechanisms involving permeability enhancement in salt through microcrack propagation and dissolution have been studied. This process has been shown to correlate linearly with the elastic properties of salt for pressure differences of up to 20 MPa (Falcon-Suarez et al., 2024). Since pressure solution can elongate the borehole cross-section in the same direction as borehole closure, these mechanisms may act synergistically, mutually reinforcing one another. A key conclusion is that regardless of which mechanism dominates, the direction of borehole elongation should remain the same analogous to classic breakouts (BB). Therefore, we conclude that the orientation of BBL-type structures can be used to infer the direction of present-day stress acting within the salt deposits.

SALT DISSOLUTION

Another potential cause of directional borehole elongation is differential dissolution of the borehole wall. Undersaturated drilling fluids enhance salt dissolution, and this effect can intensify in zones where microcracks develop particularly in the direction of S_{hmin}, where shear stresses at the borehole wall are highest. Mechanisms involving permeability enhancement in salt through microcrack propagation and stress-assisted dissolution have been documented, with dissolution rates correlating linearly with the elastic properties of salt for pressure differences up to 20 MPa (Falcon-Suarez et al., 2024). As a consequence, this process may elongate the borehole cross-section in the same direction as BB.

CAUSES OF ANISOTROPY IN NATURAL HORIZONTAL STRESSES IN SALT FORMATIONS

For the purpose of our analysis, we consider three main factors that may induce anisotropy in horizontal stresses within the salt units:

- Tectonic stresses, which in the substratum of the FSH have a NNW–SSE orientation and may locally rotate towards N–S in its eastern segment, east of the Solec-Jarocin fault.
- Differences in lithostatic pressure in the salt layers located at various depths within the FSH and in adjacent basins. Stresses generated in this manner should result in S_{Hmax} orientations roughly aligned with the dip of the homocline, NNE–SSW, or rotating towards the NE–SW, in the direction of the deepest part of the Łódź Trough (Figs. 2 and 8).
- The gravitationally driven mobility of competent layers within the salt or overlying the salt. Our previous analyses demonstrated that, in Ca2, extension is generated in the direction of the FSH dip, resulting in S_{Hmax} being reoriented to an approximately latitudinal (E–W) position.

Additionally, the influence of the local morphology of the salt base should be taken into account, as it may enhance pressure gradients in the salt and disturb the regional pressure variation trend in the FSH. The impact of this factor may be limited due to the pinching out of the oldest Na1 salt layers above the largest Ca1 reefs and A1 platforms, which reduces relief in the younger salt cyclothems (PZ2–PZ4). Since the three primary factors can generate horizontal stresses in three distinct directions – namely, NNW–SSE, NNE–SSW, and W–E – the observed orientation of BBL structures may provide insight into which factor dominates in a given location.

In boreholes where salt occurs at a depth of ~2 km, lithostatic pressure may reach ~48 MPa, increasing to ~84 MPa at 3.5 km, and exceeding 120 MPa in the Łódź Trough at depths >5 km. Such contrasts in lithostatic load may result in lateral pressure differences within each salt layer of up to 80 MPa. This can be approximated by an average horizontal pressure gradient of ~1 MPa/km. A gradient of this magnitude may promote strain decoupling within the salt relative to the deformation of the competent layers. However, due to the rheological properties of salt, even such a large pressure difference is not expected to generate significant shear stresses, which as shown in the previous section should not exceed 1 MPa within the FSH salt units.

The compilation of S_{Hmax} orientations based on BBL structures in the salt shows a statistically dominant ENE–WSW trend, identified in 14 boreholes. The average S_{Hmax} orientation in salt for all boreholes is closer to a NE–SW direction. This difference results from a systematic deviation of individual orientations from the dominant trend, shifting in the direction of the regional dip of the FSH. Since the dominant S_{Hmax} orientation is perpendicular to the regional tectonic S_{Hmax} direction, we can immediately rule out tectonic stress as a potential factor controlling the stress field in the salt. The average S_{Hmax} orientation also deviates by ~25° from the general dip of the FSH (Fig. 9). Notably, the dominant S_{Hmax} trend lies close to the bisector of the angle between the FSH dip direction and the S_{Hmax} direction within the Main Dolomite (Ca2), which constitutes a competent interlayer above salt basements such as Ca1 reefs and A1 platforms. The boreholes that show the ENE–WSW S_{Hmax} orientation are situated directly above these structural highs.

This observation suggests that the S_{Hmax} direction in the salt may result from the combined effect of the regional lithostatic pressure gradient (slightly deflected towards the deepest part of the Łódź Trough) and the kinematics of gravitational sliding of the dense Ca2 plate within the salt layers, possibly accompanied by sliding of the overlying Mesozoic cover down the inclined surface of the FSH. In this scenario, wells located closest to the deep Łódź Trough should show a NE–SW orientation of S_{Hmax}. However, only two out of four such boreholes show this trend. Therefore, our explanation of the mechanisms controlling S_{Hmax} orientation in the salt remains hypothetical.

CONCLUSIONS

To date, the orientation of borehole cross-section elongation in salt deposits has not been investigated on a regional scale. Our study, which was based on six-arm caliper logs from 23 boreholes located across the FSH showed that the borehole cross-section in Zechstein salt is systematically enlarged relative to the nominal diameter in all directions and is often distinctly elongated. The borehole enlargement, expressed as the difference between the minimum and nominal diameters, reaches up to 30 cm, with an average of ~10 cm. This phenomenon is attributed to the dissolution of salt by an undersaturated drilling mud filtrate.

In all the boreholes investigated, we also identified intervals in which directional borehole elongation (ovality) ranged from 6 to 15%, with an average of 8%. We hypothesize that this ovality results from both dissolution and closure of the borehole under anisotropic horizontal stress, and refer to these features as BBL. BBL orientations show considerable consistency in specific areas. For example, in nine boreholes located above a branching A1 platform in the western FSH, a stable ENE–WSW S_{Hmax} orientation was identified. This trend also dominates in five additional boreholes across the entire FSH. Additionally, most of identified S_{Hmax} orientations align with the FSH dip direction, but in four boreholes, it matches the regional tectonic S_{Hmax} direction. Dissolution appears to dominate over possible borehole closure since no minimum diameter in any borehole fell below the nominal diameter.

We attribute the BBL orientations to the anisotropy of horizontal stresses in the salt. Due to the relatively high heat flow in the FSH and the significant depth of the salt intervals (2–3.5 km), we estimate that the stress relaxation mechanism in the salt results in a stress drop of <1 MPa. This differential stress can produce a circumferential stress variation of 4 MPa around the borehole wall.

Considering the difference between the lithostatic pressure of the salt deposit and the hydrostatic pressure of the borehole, we estimated the maximum shear stress to be 23 MPa in shallow boreholes and 32.5 MPa in deep boreholes. These values are comparable to the uniaxial compressive strength of salt in the FSH, but are over three times lower than the confined compressive strength under borehole pressure conditions. This suggests that macroscopic breakouts or tensile fractures induced by drilling cannot form in FSH salts. However, we argue that cataclastic deformation in at the grain scale could result in microcracking. Directional differences in microcrack density within the borehole wall could lead to differential rates of pressure solution and creep. This would ultimately produce directional BBL. The fastest dissolution direction and the compression direction both favour the same BBL trend, analogous to breakouts, supporting the use of BBL to infer S_{Hmax} orientation.

The dominant ENE–WSW S_{Hmax} direction in the salt is perpendicular to the tectonic S_{Hmax} direction (NNW–SSE), therefore tectonics can be neglected as a factor controlling the stress field in the salt. The primary factor generating anisotropic stress in the salt is most likely the variation in lithostatic pressure due to changes in salt layer depth across the FSH, which lead to an average lateral pressure gradient of ~1 MPa/km, oriented parallel to the FSH dip or deflected towards the NE–SW, in the direction of the deepest part of the Łódź Trough. The observed deviation of the dominant S_{Hmax} direction in salt from these expected trends by 25° may reflect the influence of local factors, such as an increased pressure gradient on the slopes of the Ca1 reefs and A1 platforms or/and sliding of the Main Dolomite over basement highs.

Acknowledgements. This study was conducted as part of the Polish Geological Survey program, commissioned by the Ministry of Climate and Environment and funded by the National Fund for Environmental Protection and Water Management (project PIG 22.8701.2401.00.0). The authors thank ORLEN SA for providing borehole and seismic data for this study.

REFERENCES

Araszkiewicz, A., **Figurski, M., Jarosiński, M., 2016**. Erroneous GNSS Strain Rate Patterns and their Application to Investigate the Tectonic Credibility of GNSS Velocities. Acta Geophysica, **64**: 1412–1429; https://doi.org/10.1515/acgeo-2016-0057

Beauheim, R.L., **Roberts, R.M., 2002**. Hydrology and hydraulic properties of a bedded evaporite formation. Journal of Hydrology, **259**: 66–88; https://doi.org/10.1016/S0022-1694(01)00586-8

Berest, P., Brouard, B., Durup, J., 2001. Tightness Tests in Salt-Cavern Wells. Oil & Gas Science and Technology, **56**: 451–469; https://doi.org/10.2516/ogst:2001037

Bojarski, L. (ed.), 1997. Atlas hydrochemiczny i hydrodynamiczny paleozoiku i mezozoiku oraz ascenzyjnego zasolenia wód podziemnych na Niżu Polskim 1:1 000 000 (in Polish). Państw. Inst. Geol., Warszawa.

Breunese, J., **Fokker, P.A.**, **Orlic, B.**, **van Gessel, S., 2021**. Cavern convergence and subsidence: assessment of the Heiligerlee cavern field. TNO report, TNO Vertrouwelijk, Ultrecht.

Buijze, L., **Heege, J.T.**, **Wassing, B., 2022**. Finite Element modeling of natural sealing of wellbores in salt using advanced, laboratory-based salt creep laws. In: The Mechanical Behavior of Salt X (eds. J.H.P. de Bresser, M.R. Drury, P.A. Fokker, M. Gazzani, S.J.T. Hangx, A.R. Niemeijer and C.J. Spiers): 533–544. CRC Press, Utrecht.

Carcione, J.M., **Helle, H.B.**, **Gangi, A.F., 2006**. Theory of borehole stability when drilling through salt formations. Geophysics, **71**: F31–F47; https://doi.org/10.1190/1.2195447

Cornet, J.S., **Dabrowski, M.**, **Schmid, D.W., 2018**. Long term creep closure of salt cavities. International Journal of Rock Mechanics and Mining Sciences, **103**: 96–106; https://doi.org/10.1016/j.ijrmms.2018.01.025

Cristescu, N., **Hunsche, U.**, **1998**. Time Effects in Rock Mechanics. John Wiley & Sons, Chichester.

Cyran, K., **Kowalski, M., 2021**. Shape Modelling and Volume Optimisation of Salt Caverns for Energy Storage. Applied Sciences, **11**, 423; https://doi.org/10.3390/app11010423

Cyran, K., **Toboła, T.**, **Kamiński, P., 2016**. Effect of petrological features on mechanical properties of rock salt from the LGOM (Legnica–Głogów Copper District) (in Polish with English summary). Biuletyn Państwowego Instytutu Geologicznego, **466**: 51–64; https://doi.org/10.5604/01.3001.0009.4572

Czapowski, G., **Nowacki, Ł.**, **Chełmiński, J.**, **Głuszyński, A.**, **Skowroński, L.**, **2018**. Geology of Upper Permian (Zechstein) evaporites in the central Fore-Sudetic Monocline (SW Poland) (in Polish with English summary). Przegląd Solny, **14**: 29–53.

Dadlez, R., **Marek, S.**, **Pokorski, J.**, **2000**. Geological map of Poland without Cainozoic deposits 1:1 000 000. Wydaw. Kartograficzne Polskiej Agencji Ekologicznej, Warszawa.

Dusseault, M.B., **Maury, V.**, **Sanfilippo, F.**, **Santarelli, F.J., 2004**. Drilling Through Salt: Constitutive Behavior And Drilling Strategies. Presented at the 6th North America Rock Mechanics Symposium (NARMS), Houston, Texas.

Falcon-Suarez, I.H., **Dale, M.**, **Marin-Moreno, H., 2024**. Experimental study of geophysical and transport properties of salt rocks in the context of underground energy storage. Geophysical Prospecting, **72**: 2032–2048; https://doi.org/10.1111/1365-2478.13516

Flisiak, D., 2007. Methodology of rock salt research in triaxial compression tests for underground storages design (in Polish with English summary). Górnictwo i Geoinżynieria, **31:** 179–186.

Flisiak, D., 2008. Właściwości geomechaniczne skał w wysadach solnych (in Polish). In: Ruch górotworu w rejonie wysadów solnych: 99–118. Wydaw. IGSMiE PAN, Kraków.

Fokker, P.A., **Breunese, J.N., 2022**. Single-cavern convergence for an Ellis 2-branch power-law model. In: The Mechanical Behavior of Salt X (eds. J.H.P. de Bresser, M.R. Drury, P.A. Fokker, M. Gazzani, S.J.T. Hangx, A.R. Niemeijer and C.J. Spiers): 384–394. CRC Press, Utrecht, Netherlands.

Ghanbarzadeh, S., **Hesse, M.A.**, **Prodanović, M.**, **Gardner, J.E., 2015**. Deformation-assisted fluid percolation in rock salt. Science, **350**: 1069–1072; https://doi.org/10.1126/science.aac8747

Górecki, W., **Szczepański, A.**, **Sadurski, A.**, **Hajto, M.**, **Papiernik, B.**, **Jan, S.**, **Sokołowski, A.**, **Strzetelski, W.**, **Haładus, A.**, **Kania, J.**, **Rajchel, L.**, **Feldman-Olszewska, A.**, **Wagner, R.**, **Leszczyński, K.**, **Kosakowski, P.**, **Masłowska-Kuśnierz, B.**, **Hajto, E.**, **Warzecha, M.**, **Hajto, A., Warzecha, R., 2006**. Atlas of geothermal resources of Paleozoic formations in the Polish Lowlands. AGH, Kraków.

Górski, M., Wojtkowiak, Z., Radecki, S., 1999. Barnówko – Mostno – Buszewo (BMB): the largest crude oil deposit in Poland. Petroleum Geoscience, **5**: 5–15; https://doi.org/10.1144/petgeo.5.1.5

Heidbach, O., **Rajabi, M.**, **Lammers, S.**, **Morawietz, S.**, **von Specht, S.**, **Ziegler, M.**, **Reiter, K.**, **Di Giacomo, D.**, **Harris, J., Storchak, D., 2025**. The new World Stress Map database release 2025. GFZ Data Services. Data Collection; https://doi.org/10.5880/WSM.2025.001

Jackson, M.P.A., **Hudec, M.R., 2017**. Salt Tectonics: Principles and Practice. Cambridge University Press.

Jarosiński, M., 1994. Methods for measuring recent tectonic stress in the Earth's crust in deep boreholes (in Polish with English summary). Przegląd Geologiczny, **42**: 564–569.

Jarosiński, M., 1998. Contemporary stress field distortion in the Polish part of the Western Outer Carpathians and their basement. Tectonophysics, **297**: 91–119; https://doi.org/10.1016/S0040-1951(98)00165-6

Jarosiński, M., 1999. Badania współczesnych naprężeń skorupy ziemskiej w głębokich otworach wiertniczych w Polsce metodą analizy struktur breakouts (in Polish). Instrukcje i Metody Badań Geologicznych, **56**.

Jarosiński, M., 2005. Ongoing tectonic reactivation of the Outer Carpathians and its impact on the foreland: Results of borehole breakout measurements in Poland. Tectonophysics, **410**: 189–216; https://doi.org/10.1016/j.tecto.2004.12.040

Jarosiński, M., 2006. Recent tectonic stress field investigations in Poland: a state of the art. Geological Quarterly, **50** (3): 303–321.

Jarosiński, M., **Beekman, F.**, **Bada, G., Cloetingh, S., 2006**. Redistribution of recent collision push and ridge push in Central Europe: insights from FEM modelling. Geophysical Journal International, **167**: 860–880; https://doi.org/10.1111/j.1365-246X.2006.02979.x

Jarosiński, M., **Bobek, K.**, **Głuszyński, A., Durkowski, K., 2021**. Present-day tectonic stress from borehole breakouts in the North-Sudetic Basin (northern Bohemian Massif, SW Poland) and its regional context. International Journal of Earth Sciences, **110**: 2247–2265; https://doi.org/10.1007/s00531-021-02073-1

Jarosiński, M., Bobek, K., Wojtowicz, M., Wyglądała, M., Kępiński, M., 2024. Are the Carpathians tectonically active?: Geomechanical study in deep boreholes in the outer Carpathians (Poland). Tectonophysics, **890**, 230505; https://doi.org/10.1016/j.tecto.2024.230505

Karnkowski, P., 1999. Oil and gas deposits in Poland. Geosynoptics Society, Kraków.

Kiersnowski, H., Peryt, T.M., Buniak, A., Mikołajewski, Z., 2010. From the intra-desert ridges to the marine carbonate island chain: middle to late Permian (Upper Rotliegend-Lower Zechstein) of the Wolsztyn-Pogorzela High, west Poland. Geological Journal, **45**: 319–335; https://doi.org/10.1002/gj.1189

Kim, C.M., 1988. Field Measurement of Borehole Closure Across Salt Formation: Implementation to Well Cementing. Presented at the SPE Annual Technical Conference and Exhibition, Houston, Texas.

Kirsch, G., 1898. Die Theorie der Elastizität und die Bedürfnisse der Festigkeitslehre. Zeitschrift des Vereines deutscher Ingenieure, **42**: 797–807.

Kłeczek, Z., Zelias, D., 2012. Naukowe podstawy i praktyczne zasady budowy w Polsce podziemnego składowiska odpadów niebezpiecznych (in Polish). Komag, Gliwice.

Levi, N., **Habermueller, M.**, **Exner, U.**, **Piani, E.**, **Wiesmayr, G., Decker, K., 2019**. The stress field in the frontal part of the Eastern Alps (Austria) from borehole image log data. Tectonophysics, **769**, 228175; https://doi.org/10.1016/j.tecto.2019.228175

Li, S., Urai, J., 2016. Rheology of rock salt for salt tectonics modeling. Petroleum Science, **13**: 712–724; https://doi.org/10.1007/s12182-016-0121-6

Lux, K.-H., 2009. Design of salt caverns for the storage of natural gas, crude oil and compressed air: Geomechanical aspects of construction, operation and abandonment. Geological Society Special Publications, **313**: 93–128; https://doi.org/10.1144/SP313.7

Morales Salazar, J.P., 2024. Rheology of Salt Rocks. In: Drilling Geomechanics in Naturally Fractured Reservoirs Near Salt Structures: From Pore-Pressure in Carbonates to Multiphysics Models (ed. J.P. Morales Salazar): 87–128. Springer Nature Switzerland, Cham.

Munson, D.E., Dawson, P.R., 1980. Salt-constitutive modeling using mechanism maps. Sandia National Labs., Albuquerque, NM (USA); Cornell Univ., Ithaca, NY (USA). Dept. of Mechanical and Aerospace Engineering, Report number SAND-81-2196C

Peryt, T.M., **Geluk, M.C.**, **Mathiesen, A.**, **Paul, J.**, **Smith, K., 2010**. Zechstein. In: Petroleum Geological Atlas of the Southern Permian Basin Area (eds. J.C. Doornenbal and A.G. Stevenson): 123–147. EAGE Publications b.v., Houten.

Preece, D.S., 1987. Borehole Creep Closure Measurements And Numerical Calculations At the Big Hill, Texas SPR Storage Site. Presented at the 6th ISRM Congress, Montreal, Canada.

Ramesh Kumar, K., **Makhmutov, A.**, **Spiers, C., Hajibeygi, H., 2021**. Geomechanical simulation of energy storage in salt formations. Scientific Reports, **11**, 19640; https://doi.org/10.1038/s41598-021-99161-8

Spiers, C.J., **Schutjens, P.M.T.M.**, **Brzesowsky, R.H.**, **Peach, C.J.**, **Liezenberg, J.L., Zwart, H.J., 1990**. Experimental determination of constitutive parameters governing creep of rocksalt by pressure solution. Geological Society Special Publications, **54**: 215–227; https://doi.org/10.1144/GSL.SP.1990.054.01.21

Szewczyk, J., Gientka, D., 2009. Terrestrial heat flow density in Poland – a new approach. Geological Quarterly, **53** (1): 125–140.

Tackie-Otoo, B.N., **Haq, M.B.**, **2024**. A comprehensive review on geo-storage of H_2 in salt caverns: Prospect and research advances. Fuel, **356**, 129609; https://doi.org/10.1016/j.fuel.2023.129609

Tomaszewska, J., 2000. Dokumentacja badań sejsmicznych 3D rejon: Różańsko – Barnówko – Lubiszyn – 3D (reinterpretacja) (in Polish). Geofizyka Toruń Sp. z o. o., Toruń.

Urai, J.L., **Spiers, C.J.**, **Zwart, H.J.**, **Lister, G.S.**, **1986**. Weakening of rock salt by water during long-term creep. Nature, **324**: 554–557.

Wagner, R., 1998. Zechstein thickness. In: Palaeogeographical Atlas of the Epicontinental Permian and Mesozoic in Poland 1:2 500 000 (eds. R. Dadlez, S. Marek and J. Pokorski). Wydaw. Kartograficzne Polskiej Agencji Ekologicznej, Warszawa.

Zdanowski, P., Solarski, T., 2018. Hydrocarbon Plays from West Poland: Zechstein Limestone and Main Dolomite. Presented at the Underexplored Plays – Part III, Stravanger, Norway.